Electronic Structure of Genomic DNA: A Photoemission and X-ray Absorption Study

Kurt Kummer,[†] Denis V. Vyalikh,[†] Gianina Gavrila,[‡] Alexei B. Preobrajenski,[§] Alfred Kick,[||] Martin Bönsch,[||] Michael Mertig,*[,||] and Serguei L. Molodtsov*[,†]

Institut für Festkörperphysik, Technische Universität Dresden, 01062 Dresden, Germany, Helmholtz-Zentrum Berlin für Materialien und Energie - Speicherring BESSY II, Albert-Einstein-Straβe 15, 12489 Berlin, Germany, MAX-lab, Lund University, Box 118, 22100 Lund, Sweden, and Arbeitsgruppe BioNanotechnologie und Strukturbildung, Max-Bergmann-Zentrum für Biomaterialien und Institut für Werkstoffwissenschaft, Technische Universität Dresden, 01062 Dresden, Germany

Received: February 11, 2010; Revised Manuscript Received: June 18, 2010

The electronic structure of genomic DNA has been comprehensively characterized by synchrotron-based X-ray absorption and X-ray photoelectron spectroscopy. Both unoccupied and occupied states close to the Fermi level have been unveiled and attributed to particular sites within the DNA structure. A semiconductor-like electronic structure with a band gap of ∼2.6 eV has been found at which the π and π^* orbitals of the nucleobase stack make major contributions to the highest occupied and lowest unoccupied molecular orbitals, respectively, in agreement with previous theoretical predictions.

Introduction

Although the chemical structure and the morphology of DNA have been known for more than half a century[1−3] and since their discovery the DNA molecule has intensively been investigated with regard to its biological function for both in vivo and in vitro nanotechnological applications, one specific physical property of the molecule important for both fields has not been entirely revealed yet. This concerns the structure of the electronic states governing the electronic properties of the DNA molecule. Without detailed and reliable information on the electronic structure of DNA, many related issues cannot satisfactorily be addressed. On one hand, understanding the electronic properties is important for understanding DNA repair mechanisms in biological cells.[4] On the other hand, the mechanism of charge transport along the DNA molecule, in general, and, in particular, which molecular orbitals might be involved are still open questions.[5−7] The latter is essential for nanotechnological applications, where DNA molecules are proposed to be exploited as electrical conducting molecular wires.[8,9]

There have been a number of theoretical studies on the electronic structure of DNA,[10−12] but comprehensive experimental data are still lacking. Some attempts to determine the electronic properties of DNA have been undertaken by means of scanning tunneling spectroscopy and direct measurements of the electrical conductivity.[8,13−17] However, the obtained results differ significantly, and it is very difficult to shape a uniform picture from them. Depending on the specific experimental setup and the sample prepreparation process, DNA has been found insulating,[9] semiconducting,[13−16] and conducting,[8,13] and even superconductivity below 1 K has been reported.[18] Here, photoemission (PE) and X-ray absorption spectroscopy may give a deeper insight since they address the electronic states directly.

So far, PE studies on DNA duplexes and specific building blocks of DNA, in particular the nucleobases, have been mainly focused on the core-level states.[19−22] However, high-quality spectra which allow for a conclusive decomposition of the four DNA-relevant PE lines, i.e., the C 1s, N 1s, O 1s, and P 2p lines, are rare[19] or in the case of double-stranded DNA still missing. Especially, detailed discussion and quantitative analysis of all core level spectra including the subcomponents would be very helpful for the chemical analysis and characterization of DNA samples. Also, valuable near-edge X-ray absorption fine structure (NEXAFS) data have been published for the nucleobases,[22−26] but high-quality data for double-stranded DNA molecules are still missing. Moreover, no attempts have been undertaken to determine the energies of the involved unoccupied molecular orbitals so far, which could help to experimentally identify the lowest unoccupied molecular orbitals and their locations in the DNA double helix. The same holds for the valence states, where contributions of the nucleobases to the highest occupied molecular orbital have been theoretically predicted,[10,11] but the experimental verification of these predictions is still missing.

Here, we present a comprehensive experimental study of the electronic structure of genomic DNA covering core-level energy shifts as well as the occupied and unoccupied molecular states close to the Fermi level (E_F). With these investigations, we will close many of the above-mentioned gaps in the current knowledge on the electronic structure of double-stranded DNA. Highly resolved X-ray PE data presented here allow reliable distinction and assignment of the different components in all relevant core-level spectra. Their quantitative analysis verifies all details of the chemical structure of DNA and, thus, proves intactness of the studied DNA molecules. NEXAFS spectroscopy at the C 1s, N 1s, O 1s, and P 2p threshold reveals manifold transitions into various unoccupied molecular orbitals which are all identified including their binding energies (BEs). Contributions of the nucleobases to the highest occupied molecular orbitals are demonstrated by means of resonant PE spectroscopy. The obtained result extends the present knowledge about the largely understood electronic structure of the nucleobases to entire DNA strands.

* To whom correspondence should be addressed. E-mail: michael.mertig@tu-dresden.de; molodtso@physik.phy.tu-dresden.de.
[†] Institut für Festkörperphysik, Technische Universität Dresden.
[‡] Helmholtz-Zentrum Berlin für Materialien and Energie - Speicherring BESSY II.
[§] Lund University.
[||] Max-Bergmann-Zentrum für Biomaterialien and Institut für Werkstoffwissenschaft, Technische Universität Dresden.

10.1021/jp1013237
Published on Web 07/07/2010

Experimental Section

The experiments were conducted at the Berliner Elektronenspeicherring für Synchrotronstrahlung (BESSY) using radiation from the Russian-German Beamline (RGBL)[27,28] and, in parts, repeated at bending-magnet beamline D1011 located at the MAX II storage ring of MAX-lab (Lund, Sweden). These beamlines provide moderate photon flux distributed continuously over a wide photon energy range and are, therefore, particularly suitable for radiation sensitive biological molecules.[29−33] Films of doubled-stranded salmon testes DNA (GC content 41.2%) with an average length of 2000 base pairs, that had been deposited onto a Si substrate covered with a ∼100 nm thick gold layer, served as samples. Further experimental details are available as Supporting Information.

Results and Discussion

Core-Level Structure. ***Binding Energies and Assignment.*** Our study of the electronic structure of DNA molecules starts with an investigation of the different core-level states, i.e., the C, N, and O 1s as well as the P 2p. To this end, we investigated the deposited DNA layer by X-ray photoemission spectroscopy (XPS). Note that a profound knowledge of the core-level structure will be required later on for the characterization of the unoccupied electronic states above E_F by means of NEXAFS spectroscopy. This is because the detected excitation energies for 1s electron transitions into these states depend on both the initial 1s state energy as well as the final state energies.

Moreover, knowing the core-level binding energies allows for a detailed chemical analysis of the samples. At that, one makes use of the fact that the chemical state of an atom depends on its neighbors and, in particular, on their electronegativities. The latter strongly affects the spatial distribution of the valence electrons which concentrate in the vicinity of highly electronegative sites. As a consequence, the particular 1s binding energy differs for different surroundings due to ground state charge transfer (initial-state effect) and core-hole screening (final-state effect). This effect is commonly denoted as chemical shift and the basis for chemical analysis via electron spectroscopy.[34] We are fully aware of the possible influence of final state effects on BEs in general. However, considering previous experiments on protein layers,[29,30] we presume that the chemical shift in biomolecules like DNA is governed by the ground-state charge transfer. Therefore, the chemical analysis based upon comparison of the molecular structure of DNA (Figure 1) with the measured XPS spectra can be used to verify that the deposited DNA molecular film has the expected chemical composition.

An XPS overview spectrum taken with a photon energy of 600 eV is shown in Figure 2a. This photon energy enables us to probe a wide range of binding energies containing all significant core levels. In addition to the Au 4f signal of the underlying gold substrate, four intense PE lines appear in the overview spectra which were identified as the signals from the C 1s, N 1s, O 1s, and P 2p core levels, respectively. Apart from hydrogen, which cannot be detected via XPS, these are the only four elements contained in DNA molecules. Subsequently, detailed PE spectra of these four core levels were recorded with a higher density of measuring points and exploited for the chemical analysis of the samples. All spectra were aligned thoroughly in binding energy by referencing them to the Au $4f_{7/2}$ peak of the polycrystalline gold substrate which was set to 84.0 eV.

The C 1s core-level PE spectrum (Figure 2b) reveals a manifold structure which consists of several distinguishable PE components. This reflects the complex chemical structure of DNA molecules where carbon atoms are found in a variety of bonds. Least-squares fit analysis grants insight into the detailed structure of the C 1s PE spectrum. Its contour is reproducible with the help of four individual peaks (I−IV), in agreement with previous reports on nucleobases and DNA.[19,20,35] The above-mentioned initial state argumentation based on electronegativities has led us to the assignments presented in Table 1: component I at 285.0 eV BE corresponds to pure carbon and hydrocarbon environments, i.e., C−C and C═C. When a more electronegative oxygen or nitrogen atom binds to a carbon, it contributes to component II. Of course, one cannot expect fully identical BEs for C−N and C−O type carbon atoms, but they are supposed to differ insignificantly in BE. Nonetheless, due to the only minor difference, we regard it as justified to assign both chemical environments to component II. Moreover, using a different peak for each of them in the fit analysis would be far beyond the scope of our experimental resolution and, hence, not conclusive. If both oxygen and nitrogen are bound to a carbon atom, the latter will either contribute to the PE component III or IV (cf. Table 1).[20,35−37]

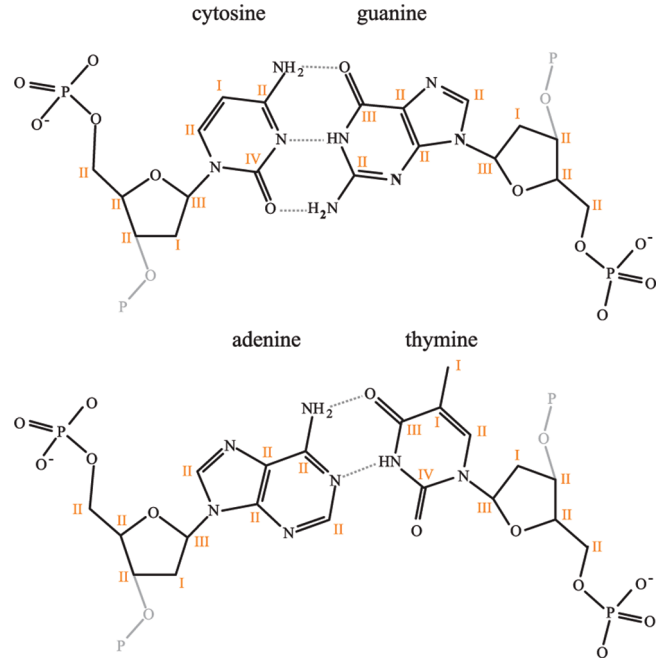

Figure 1. Chemical structure of d(G)−d(C) and d(A)−d(T) base pairs together with the corresponding backbone segment of the DNA double strand. The carbon atoms are marked with the Roman number of the PE component in Figure 2b to which they contribute (cf. also Table 1).

Fit analysis of the N 1s PE signals (Figure 2c) reveals two components, A and B, at BEs of 399.1 and 400.7 eV. The O 1s spectrum (Figure 2d) is well described assuming two components C and D at 531.4 and 533.1 eV BE. Again, our electronegativity-based assignment (Table 1) is in good agreement with experimental results and calculations published previously.[36−40]

Since phosphorus is only found in the phosphate groups (PO_4^-) of the backbone, the P 2p PE line shows a simple doublet line shape (Figure 2e). It was best fitted assuming a spin−orbit split of 0.92 eV between the $2p_{3/2}$ and the $2p_{1/2}$ component with the former located at a BE of 133.8 eV. The intensity ratio between the $j = 3/2$ and $j = 1/2$ component (3.8:2) agrees well with the one expected from the respective m_j degeneracies (4:2). The

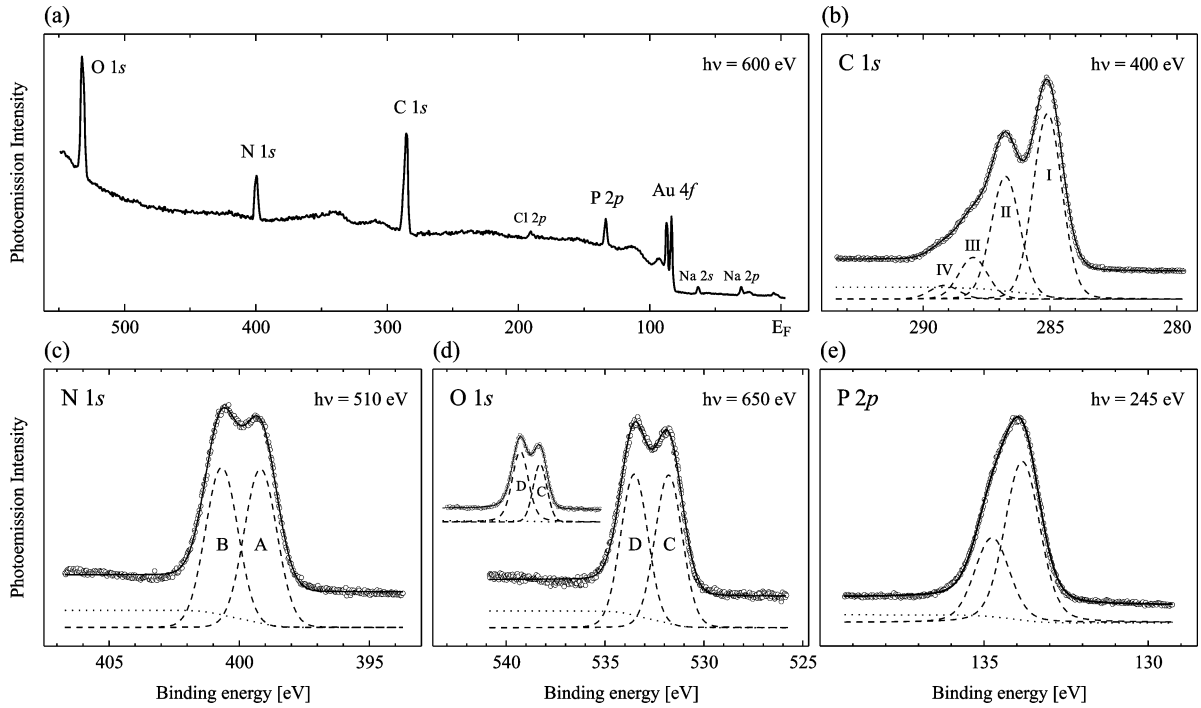

Figure 2. Overview and high-resolution core-level PE spectra together with results of the fit analysis. Assignment of the PE components I−IV and A−D is discussed in the text and summarized in Table 1. The inset in (d) shows an example of the occasionally observed enhancement of PE component D which we explain by the interaction of H^+ ions with backbone phosphate groups (for details, see text).

TABLE 1: Binding Energies of the PE Components in Figure 2 Together with the Assigned Chemical Structures[a]

core level		BE [eV]	chemical group	relative PE intensity	relative occurrence
C 1s	I	285.0	C−C, C═C	51.0	18.3
	II	286.6	C−O, C−N, C−NH_2, N−C−N, N═C−N	33.8	61.3
	III	288.0	N−C−O, N−C(═O)−C	11.4	15.3
	IV	289.2	N−C(═O)−N	3.8	5.1
N 1s	A	399.1	C−NH_2, C═N−C	49.8	54.0
	B	400.7	N−C−O, N−C═O	50.2	46.0
O 1s	C	531.6	C═O, P═O, P−O^-···Na^+	49.8	50.0
	D	533.3	C−O−P, C−O−C	50.2	50.0
P $2p_{3/2}$		133.8	PO_4^-	-	-

[a] In the last two columns, the relative PE intensity of each component is compared with the relative occurrence of the assigned atom type in salmon testes DNA.

found values do resemble tabular values and previous experimental data for DNA layers.[19]

Quantitative Analysis. We will now turn to a quantitative analysis, at which we compare the relative abundance of chemical groups with the relative intensity of the respective PE component. To do so, we built an "averaged base-pair" block by weighting the adenine-thymine (AT) and the guanine-cytosine (GC) base pairs with their relative share in the DNA investigated, i.e., 41.2% for GC and 58.8% for AT. This averaged block contains, e.g., 19.6 carbon atoms, of which 3.6, 12, 3, and 1 contribute to C 1s PE component I, II, III, and IV, respectively.

For the N 1s and O 1s spectra, both DNA stoichiometry and PE intensity are in excellent agreement. For the O 1s spectrum, however, we occasionally observed a notable deviation from the shape shown in Figure 2d. Then the intensity of the component C was reduced down to 45%, in one case even down to 37% (cf. inset in Figure 2d). There might be several explanations for this observation. One possible reason could be the adsorption of atmospheric oxygen or oxides to the surface. However, the corresponding O 1s PE signals are usually detected at lower BEs[41,42] which would cause a relative enhancement of C rather than a reduction or even the appearance of a third spectral component below 531 eV. Also, the presence of carbon oxides would cause a change in the C 1s line shape to an extent similar to that in the O 1s spectrum which was not detected. Moreover, extensive oxidation of the gold surface at room temperature is, in general, not expected. Radiation damage could probably be excluded as a likely cause for the occasional differences in the O 1s spectra, too, because there was no detectable influence of the time of irradiation on the O 1s spectral shape for irradiation times of 1 h and more.

We suppose that the DNA preparation could be responsible for the occasional enhancement of PE component D. One can assume that the negative charge of the DNA backbone is usually entirely compensated by the Na^+ ions being in the sodium salt solution from which the samples were prepared. Indeed, respective Na 2s and 2p PE lines at ∼64 eV and ∼32 eV BE, respectively, show up in the overview spectrum (Figure 2a). Moreover, given their low cross section at $h\nu = 600$ eV—approximately 5 times lower than the P 2p cross section and 9 times lower than the Cl 2p cross section[43]—the Na concentration seems comparable to that of the phosphate groups and, in light of the low Cl 2p PE intensity at 193 eV, only to

a small part explained by traces of remaining sodium chloride. We assume that the occasional redistribution of PE intensity from component C to D is observed, and when in the dried sample, the backbone charge may not entirely be compensated by Na^+ ions but instead in parts by H^+ ions stemming from the aqueous solution, too. In this case, the claim of the counterion to the surplus electron of the $P-O^-$ segment would probably be much larger[44] which could possibly affect the O 1s BE in the ground state or the core hole screening in the PE final state or both, thus leading to the observed enhancement of the high-BE component D. Within that scenario, the relative intensity of PE component C could be lowered to 33%, corresponding to a situation where H^+ counterions compensate the entire backbone charge. Our experimental data vary within this range and may indicate that occasionally the backbone charge is not entirely neutralized by sodium but partly by H^+ ions, too.

The found general consistency of DNA stoichiometry and PE intensity distribution is a proof that the deposited DNA has the expected chemical composition. Another probe for the sample quality is the P/N ratio.[19] Since phosphorus is found solely in the DNA backbone whereas only the nucleobases contain nitrogen, the P/N PE intensity ratio can also be exploited to demonstrate the integrity of the DNA molecules. Because changing of the photon energy can cause shifting of the beam position on the sample, we decided to record the P 2p and N 1s spectra with the same photon energy of 510 eV, assuming that the mean escape depth within the DNA layer is basically the same for P 2p and N 1s electrons. After normalization to the subshell photoionization cross section and the storage ring beam current, we, thus, obtained an experimental P/N ratio of 0.29 which is in excellent agreement with the calculated value of 0.27.

While N 1s, O 1s, and P 2p PE signals as well as the P/N ratio are in convincing agreement with calculations based on the DNA molecule stoichiometry, there is a remarkably high discrepancy in the case of C 1s PE. Considering the reasonable accordance between the intensity ratio of the PE components IV:III:II amounting to 1:3:10 and the calculated 1:3:12, this discrepancy is partly repealed. Nonetheless, the fact remains that PE component I at 285.0 eV is unexpectedly intense. This effect of an increased C−C like content in DNA samples is also visible in previously published spectra.[19,45] Since the rest of the XPS data is in good agreement with the expectations based on the DNA stoichiometry, we assume that the presence of undesired carbon compounds on the substrate is responsible for this unexpected C−C signal. Blank gold substrates that have undergone all steps of the sample preparation except for the actual DNA deposition also showed a C 1s PE signal, in the form of a singlet peak at 285.0 eV BE. However, the corresponding C 1s NEXAFS spectra revealed almost no structure in the interesting π^* region. Therefore, these carbon contaminations should not affect further analysis.

Unoccupied Electronic States. ***X-ray Absorption Resonances.*** The electronic properties of a molecule are governed by the electronic states near the Fermi level. PE spectroscopy can probe the occupied states below E_F but cannot access unoccupied states above. However, the latter are accessible by X-ray absorption spectroscopy. We studied element- and symmetry-specific unoccupied electronic states on the basis of the near-edge X-ray absorption fine structure (NEXAFS) at the C 1s, N 1s, O 1s, and P 2p threshold, respectively.

The π^* regions of the NEXAFS are interpreted qualitatively within a simple "building block" model.[46] In doing so, specific NEXAFS features are attributed to characteristic chemical

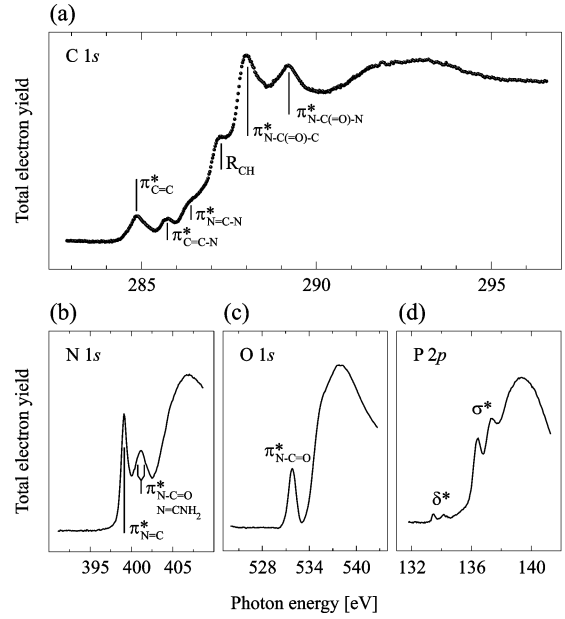

Figure 3. NEXAFS of the four relevant absorption thresholds. Assignment of the observed resonances is based on the building block model. For details, see text.

groups of DNA, and the total spectrum is considered as a superposition of the elementary spectra of these groups. This approach is most promising for molecules with predominantly nonconjugated, localized bonds between the utilized building blocks. Although interactions between the building blocks are generally neglected, this simplified model should yield reliable results since the available data on DNA substructures, and in particular the nucleobases, are fairly comprehensive and allow us to work with sufficiently large building blocks that already include most of the conjugation effects. Moreover, the building block approach has already been applied to DNA substructures successfully.[23]

Figure 3a shows the C 1s NEXAFS spectrum originating from transitions into unoccupied 2p-derived electronic states. It reveals a rather complex structure due to the diversity of molecular orbitals involving carbon atoms. The region between 284 and 290 eV is mainly characterized by sharp transitions into π^* symmetry orbitals, whereas the σ^* resonances above 290 eV are very broad due to very short lifetimes of the corresponding core-exited states.[47] We will not discuss the σ^* transitions here because the respective orbitals lie far above the Fermi level and contain only little information on chemical and electronic properties of the molecules.

Observations for amino acids,[48] proteins,[49] polymers,[50] and DNA nucleobases[22,23,26] revealed that the resonances at 285.0, 285.9, and 286.6 eV correspond to C 1s $\rightarrow \pi^*$ transitions within the aromatic C═C, C═C−N, and N−C═N structures, respectively. It was shown by both calculations and measurements that the 285.0 eV resonance is unique to the nucleobase cytosine.[51] For proteins, for instance, it is well-known that the resonant photon energy for C 1s $\rightarrow \pi^*_{C=O}$ transitions strongly depends on the chemical environment of the C═O group.[52] Owing to the chemical shift of the core level, it changes from 286.6 to 288.2 eV or 289.5 eV, respectively, when one or both of the adjacent carbon atoms in the C−C(═O)−C structure are replaced by nitrogen atoms.[49,53] We therefore assign the peaks at 288.0 and 289.2 eV to $\pi^*_{N-C(=O)-C}$ and $\pi^*_{N-C(=O)-N}$ resonances, respectively. The feature at 287.3 eV has been found in a variety of organic molecules.[23,47,48,54,55] It was mostly

attributed to transitions into antibonding states of the C−H bond with σ^*-character based on a number of older publications.[56−58] More recent calculations, however, revealed a more Rydberg-like character.[59,60]

The N 1s NEXAFS spectrum in Figure 3b shows two sharp π^* resonances at photon energies of 399.1 and 401.1 eV, like reported previously for other DNA samples.[61] In a number of previous reports for purine and pyrimidine bases, they were attributed to −N═ and −NH− blocks, respectively,[62,63] based primarily on an older publication by Kirtley et al.[64] and on reported ab initio calculation results.[65] However, these calculations partly deviate from experimental findings.[23] There, an intense 399.1 eV peak was found in the adenine spectra. However, an also predicted intense second peak at 2 eV higher photon energy was hardly detectable. In light of the previous experimental reports on nucleobases, we propose a slightly different assignment. The large chemical shifts of the C 1s and N 1s core levels already demonstrate the strong effect of the highly electronegative oxygen on the spatial electron distribution within the carbonyl groups [N−C(═O)]. This should affect the N 1s → π^* resonance energies, too, since downshift of the core level requires higher photon energies for transitions into states at the Fermi level or closely above. Therefore, we attribute the 401.1 eV feature to N 1s → π^* resonances within carbonyl groups. This assignment is supported by previous measurements and calculations of nucleobases,[23,26] where the 401.1 eV peak was hardly present in spectra of the nucleobase adenine which lacks the carbonyl group. On the other hand, amino groups at the pyrimidine and purine rings seem to affect the π^* orbital energy, too, since adjacent ring nitrogen atoms show a blue shift in the N 1s →π^* transition energies.[65] Hence we assume that two only slightly energy separated contributions merge in the 401.1 eV peak which leads to its relatively broad shape. The strong absorption around 399.1 eV is caused by transitions starting from 1s states of the remaining nitrogen atoms in the heterocycles.[48,50]

The O 1s NEXAFS spectrum depicted in Figure 3c reveals only one rather broad π^*-derived feature with a maximum at around 531.4 eV photon energy, like it was observed before for other DNA samples.[61] Its structure can only be caused by a superposition of π^* transitions at the carbonyl site of the nucleobases cytosine, guanine, and thymine[22,26,63,66] because the sugar and phosphate groups found in the DNA backbone show notable contributions solely in the σ^* region above 235 eV.[23] At the P 2p threshold, two doublet-like features occur, each splitted by 0.9 eV (Figure 3d). We want to remind that the spin−orbit splitting of the P 2p core level values 0.92 eV. Hence, these two doublets reflect most likely transitions of $2p_{3/2}$ and $2p_{1/2}$ electrons into two different molecular orbitals of the phosphate group with σ^* and δ^* character, respectively.

In summary, we measured the NEXAFS at all four relevant absorption thresholds of the DNA molecule with high-energy resolution. Especially at the C 1s threshold we were thus able to detect and identify π^* resonances which have been overlooked so far.

Energy Levels of the Unoccupied States. We will now discuss the unoccupied states closely above the Fermi edge. With the knowledge of the core-level BEs and excitation energies for transitions into the lowest unoccupied states, one can try to obtain the energies of the latter. The simplest approach is to add the transition energies to the respective core-level BEs. In general, the situation is complicated by the fact that the final states in XPS and NEXAFS differ considerably and so do the relaxation energies transferred to the excited electron. In the near-edge X-ray absorption process, the core-level electron is excited directly into a screening orbital, whereas the photoemission process leaves behind a system with one electron less and the screening orbital unoccupied.

For low-Z molecules[67] like DNA, however, spatial overlap between molecular orbitals is comparatively high, and a valence electron of the adjacent atoms will occupy the screening orbital almost immediately during the PE process. Therefore, as a first approximation the final states measured by XPS and NEXAFS can be assumed to be comparable. Furthermore, at least for the three consecutive elements carbon, nitrogen, and oxygen, the impact of the 1s core hole on the states under observation should be comparable. A third aspect is the highly covalent character of all considered bonds with the only exception of the ionic binding of the Na^+ counterions to the backbone. Hence, energy shifting effects of Coulomb charge barriers, which are in general difficult to estimate quantitatively, can be neglected. Therefore, if the NEXAFS transitions are nonexitonic and the relaxation of the π^* orbital energies themselves due to the core hole is neglibible—which we will assume without evidence here—the simple approach proposed above will be suitable to align the NEXAFS derived unoccupied molecular orbitals on a common energy scale with PE derived results.

In Figure 4a we illustrate our approach at the example of the $\pi^*_{N-C=O}$ orbital. By adding the transition energies, detected for this orbital in the three relevant NEXAFS spectra, to the respective C 1s, N 1s, and O 1s BEs measured with XPS, we find an energy for the $\pi^*_{N-C=O}$ orbital in each case. More precisely, we do both: (i) alignment of the NEXAFS spectra relative to each other with respect to the measured energy separation of the excited core levels and (ii) alignment of the spectra on the PE energy scale with E_F of the gold substrate as a reference point. Clearly, the positions of the $\pi^*_{N-C=O}$ peaks coincide in the aligned spectra (dashed line in Figure 4a). This indicates (i) that the transitions though starting at different core levels all end up in the same unoccupied molecular orbital and (ii) that this orbital is found at E_F on the PE energy scale.

In this manner, all NEXAFS resonances were analyzed resulting in an energy landscape of the lowest unoccupied states as depicted in Figure 4b. Obviously, both the π^* orbitals involving either cytosine C═C bonds or C═N bonds of the pyrimidine or purine bases and the $\pi^*_{N-C=O}$ orbital lie directly at E_F. Therefore, within our experimental resolution, we cannot identify one of them as the lowest unoccupied molecular orbital (LUMO) since they are separated in energy by less than 100 meV. However, all of them are found within the nucleobases stack, i.e., the "inner structure" of the DNA molecule. We are aware that the alignment of the P 2p NEXAFS features might be somewhat imprecise since in this case we deal with a 2p ground state where the effect of the core hole can possibly deviate from the 1s situation. Nevertheless, the finding that backbone derived orbitals are found far above the LUMO should not be affected by that.

Note again that, for instance, in the case of the 1s → $\pi^*_{N-C=O}$ orbital its energy was determined by combination of NEXAFS and XPS data for three different atomic sites. The fact that in all three cases the orbital energies coincide illustrates the applicability of our approach.

In summary, we found that the lowest unoccupied molecular orbitals are located in the nucleobases stack, i.e., the inner part of the DNA double strand, which is in agreement with recent calculations.[10,11] More precisely, the π^* orbitals involving cytosine C═C bonds, C═N bonds of the pyrimidine or purine bases, as well as the $\pi^*_{N-C=O}$ orbital were all found to lie

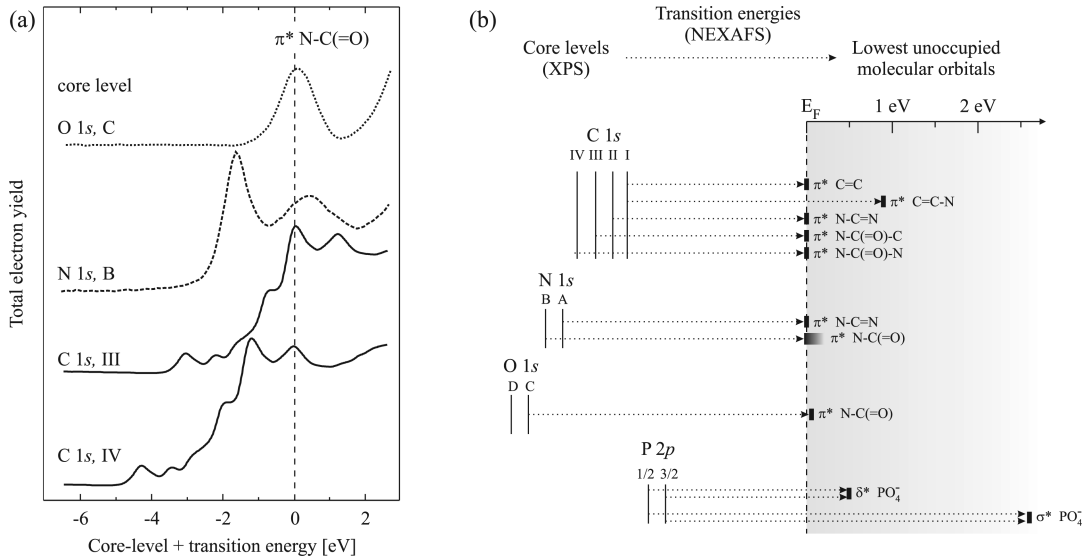

Figure 4. (a) C, N, and O 1s NEXAFS spectra aligned on the PE energy scale by adding the photon (or transition) energy scale to the particular core level BEs of each of the N−C(═O) group atoms. All $\pi^*_{N-C(=O)}$ resonances lie at the same energy, suggesting that (i) the respective transitions end up in the same orbital and (ii) this orbital is located at E_F. (b) Energy map of the lowest unoccupied molecular orbitals, obtained by combined use of XPS and NEXAFS data as shown in (a).

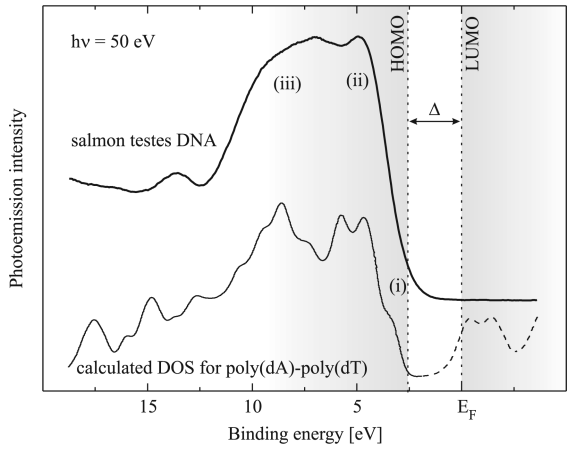

Figure 5. Valence band PE spectrum together with the density of states (DOS) calculated for a poly(dA)−poly(dT) DNA double strand.[12] The experimentally determined bandgap Δ amounts to ∼2.6 eV.

directly at E_F. Within our experimental resolution, none of them could be identified as the actual LUMO.

Valence States. Besides the knowledge of the unoccupied states, information on the valence states and their respective binding energies is needed for a full characterization of the DNA layers with regard to electronic properties. The valence band PE spectrum recorded at a photon energy of $h\nu = 50$ eV is shown in Figure 5. Energy alignment with respect to the Fermi level was done with the help of the Au $4f_{7/2}$ peak and counterchecked using the Na 2p PE peak (30.5 eV BE). Additionally, we used the "second-order" C 1s PE peak to check proper energy alignment, in particular its component I. To this end, the photon energy was tuned to 285.0 eV, and the valence band was recorded once again. Note that under these conditions the main component I of the second-order peak shall be found exactly at 0 eV BE.

Despite its complex chemical structure, the DNA molecule reveals a well-resolved valence band PE structure consisting of at least three distinct components. The PE contribution of the highest occupied molecular orbital (HOMO) is found at about 2.6 eV below the Fermi level [component (i)]. It is superimposed by two intense components at about 5 eV (ii) and 9 eV (iii) BE. Note that this general shape had shown up in previous ab initio density of states (DOS) calculations of short poly(dA)−poly(dT) DNA double strands[12] (also shown in Figure 5) and that the size of the band gap coincides with that determined in recent scanning tunneling spectroscopy (STS) studies[15] and calculations performed for nucleobases.[26,68]

However, attribution of single valence band features to certain chemical groups or orbitals solely on the basis of direct PE data is mostly complicated by the fact that valence band PE is not element-specific. In this respect, theoretical approaches can offer some help.[69] Recent calculations on DNA show that the highest occupied states derive from the π orbitals of the nucleobases, whereas contributions of the sugar−phosphate backbone to the HOMO were not found.[10,11] Calculations for proteins indicate that the components (ii) and (iii) at higher BEs are most likely σ orbital derived.[70] Beyond that, reliable theoretical data on valence states in DNA in particular and biomolecules in general are still lacking due to the rather low symmetry and periodicity and the huge unit cell of these molecules. Hence, discussion of the valence states solely on the basis of calculations still remains rather vague.

To get experimental insight into the site-specific valence state structure, we applied a resonant photoemission (ResPE) approach. In the resonant PE phenomenon, two different processes interfere with each other: (i) direct photoemission where a valence electron is excited into free continuum states and (ii) autoionization. The latter denotes a decay of the core-excited state via an Auger process, also called resonant Auger decay. The probability for transitions into unoccupied states changes drastically, when tuning the photon energy across an absorption threshold, which, in turn, leads to large variations in the overall photoionization cross section. In the case of a sufficient overlap between initial, intermediate, and final states, i.e., large degree of localization of all involved orbitals, the participator decay channel is accessible for the intermediate state leading to a site-specific enhancement of certain valence band PE components.[71]

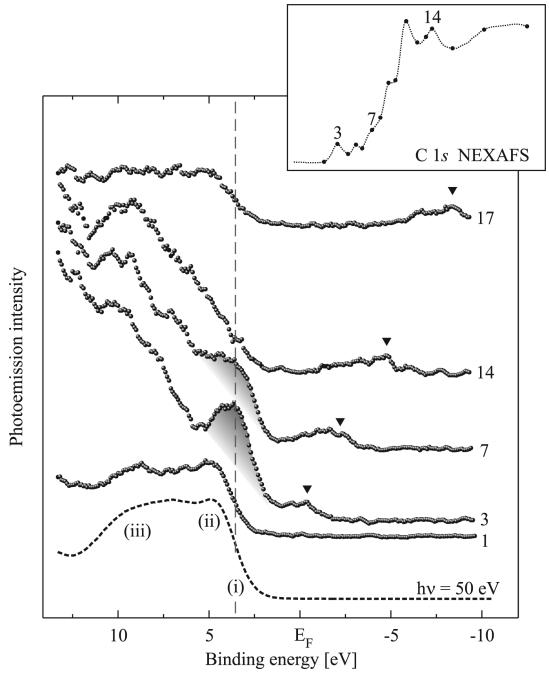

Figure 6. Resonant PE spectra recorded at the C 1s absorption threshold. Second-order contributions are marked by black triangles. Resonant enhancement of the PE component when tuning the photon energy across the $\pi^*_{C=C}$ and $\pi^*_{N-C=N}$ resonances (shaded areas in spectra 3 and 7) reveals the contribution of the $\pi_{C=C}$ and $\pi_{N-C=N}$ orbitals to the highest occupied molecular orbitals.

Carbon atoms participating in various chemical bonds are the main constituent of DNA. They are found in all structural components of DNA, i.e., the nucleobases as well as the sugar−phosphate backbone. Note that nitrogen atoms, for instance, are contained in the nucleobases only, and information obtained from N 1s ResPE data will thus be limited to the nucleobases stack, too. Therefore, we regard the ResPE approach to be most promising at the C 1s threshold, all the more since ResPE data are already available for the N 1s threshold.[72] In respect thereof, our data expands the present ResPE insight to the entire DNA molecule.

Figure 6 depicts changes in the valence band PE, when the photon energy is tuned across the C 1s threshold. For the purpose of comparison, the spectrum recorded at 50 eV photon energy is plotted as a dotted line at the very bottom of the panel. Obviously, the PE intensity of the HOMO feature is enhanced significantly when the photon energy crosses the $\pi^*_{C=C}$ and the $\pi^*_{N-C=N}$ resonances. This points not only to a contribution of the C═C and C═N bonds to the highest occupied states but also to a partly localized nature of the respective bonding and antibonding orbitals. Note that, although no strong enhancement is observed when the photon energy is tuned to the C═C−N and the two N−C(═O) resonances, this does not automatically mean that these bonds do not contribute to the HOMO feature. Instead, suppression of the participator decay channel can also be caused by a rather small spatial overlap of the involved orbitals caused by their more delocalized character or their differing orientations.[73]

Summing up, our data show that the highest occupied molecular orbitals are located in the nucleobases of the DNA double strand, similar to what has been found in previous calculations.[10,11]

Conclusions

Genomic DNA, deposited as a layer on a gold layer, was investigated by means of XPS, NEXAFS, and ResPE spectroscopy. The chemical analysis of the samples carried out by XPS verified that the deposited DNA molecular film has the expected chemical composition. NEXAFS spectroscopy revealed many unoccupied states which we were able to identify in the framework of a building blocks analysis approach. Direct and resonant PE spectroscopy gave insight into the valence band structure near E_F.

The investigated genomic DNA exhibits a semiconductor-like electronic structure with a band gap Δ of about 2.6 eV. The lowest unoccupied molecular orbitals are π^* orbitals deriving from C═C, C═N, or C═O bonds of the nucleobases stack. No contributions of the DNA backbone to the lowest unoccupied orbitals were found. Also, the π orbitals of the nucleobases make the major contribution to the highest occupied molecular orbitals. For C═C and C═N derived π and π^* orbitals, a partly localized character was demonstrated.

We believe that the presented, comprehensive report on the electronic structure of DNA is highly suitable to serve as a foundation to enter into issues like specific mechanisms of electron transfer along DNA molecules which have not been addressed satisfactorily yet. Also, although the semiconducting behavior implied by our spectroscopic data is consistent with most of what has been reported before, other studies indicate that DNA molecules could possibly become conductive, too. Further research is certainly needed to understand how far the electronic properties of long DNA strands may, for instance, depend on the sequence of the base pairs.

Acknowledgment. We would like to thank Jan Voigt for the preparation of the gold coatings and Michael Weigel for his help in the early stage of the project. This work was financially supported by the DFG (Grant Nos. MO 1049/5-1, ME 1256/7-2, ME 1256/10-1, ME 1256/12-1 and ME 1256/13-1), the BMBF (Grant No. 03WKBH2G), the SAB (Grant No. 14120/2447), and the bilateral program Russian-German laboratory at BESSY.

Supporting Information Available: Additional experimental details. This material is available free of charge via the Internet at http://pubs.acs.org.

References and Notes

(1) Watson, J. D.; Crick, F. H. *Nature* **1953**, *171*, 737.
(2) Wilkins, M. H.; Stokes, A. R.; Wilson, H. R. *Nature* **1953**, *171*, 738.
(3) Franklin, R.; Gosling, R. G. *Nature* **1953**, *171*, 740.
(4) Boon, E. M.; Livingston, A. L.; Chmiel, N. H.; David, S. S.; Barton, J. K. *Proc. Natl. Acad. Sci. U.S.A.* **2003**, *100*, 12543.
(5) Kelley, S. O.; Barton, J. K. *Science* **1999**, *283*, 375.
(6) Klotsa, D.; Römer, R. A.; Turner, M. S. *Biophys. J.* **2005**, *89*, 2187.
(7) Osakada, Y.; Kawai, K.; Fujitsuka, M.; Majima, T. *Proc. Natl. Acad. Sci. U.S.A.* **2006**, *103*, 18072.
(8) Fink, H.-W.; Schönenberger, C. *Nature* **1999**, *398*, 407.
(9) Braun, E.; Eichen, Y.; Sivan, U.; Ben-Yoseph, G. *Nature* **1998**, *391*, 775.
(10) de Pablo, P. J.; Moreno-Herrero, F.; Colchero, J.; Gómez Herrero, J.; Herrero, P.; Baró, A. M.; Ordejn, P.; Soler, J. M.; Artacho, E. *Phys. Rev. Lett.* **2000**, *85*, 4992.
(11) Artacho, E.; Machado, M.; Sánchez-Portal, D.; Ordejón, P.; Soler, J. M. *Mol. Phys.* **2003**, *101*, 1587.
(12) Wadati, H.; Okazaki, K.; Niimi, Y.; Fujimori, A.; Tabata, H.; Pikus, J.; Lewis, J. P. *Appl. Phys. Lett.* **2005**, *86*, 023901.
(13) Cai, L. T.; Tabata, H.; Kawai, T. *Appl. Phys. Lett.* **2000**, *77*, 3105.
(14) Porath, D.; Bezryadin, A.; de Vries, S.; Dekker, C. *Nature* **2000**, *403*, 635.

(15) Shapir, E.; Cohen, H.; Calzolari, A.; Cavazzoni, C.; Ryndyk, D. A.; Cuniberti, G.; Kotlyar, A.; di Felice, R.; Porath, D. *Nat. Mater.* **2008**, *7*, 68.

(16) Yoo, K.-H.; Ha, D. H.; Lee, J.-O.; Park, J. W.; Kim, J.; Kim, J. J.; Lee, H.-Y.; Kawai, T.; Choi, H. Y. *Phys. Rev. Lett.* **2001**, *87*, 198102.

(17) Endres, R. G.; Cox, D. L.; Singh, R. R. P. *Rev. Mod. Phys.* **2004**, *76*, 195.

(18) Kasumov, A. Y.; Kociak, M.; Gueron, S.; Reulet, B.; Volkov, V. T.; Klinov, D. V.; Bouchiat, H. *Science* **2001**, *291*, 280.

(19) Petrovykh, D. Y.; Kimura-Suda, H.; Tarlov, M. J.; Whitman, L. J. *Langmuir* **2004**, *20*, 429.

(20) May, C. J.; Canavan, H. E.; Castner, D. G. *Anal. Chem.* **2004**, *76*, 1114.

(21) Vilar, M. R.; Botelho do Rego, A. M.; Ferraria, A. M.; Jugnet, Y.; Nogues, C.; Peled, D.; Naaman, R. *J. Phys. Chem. B* **2008**, *112*, 6957.

(22) Plekan, O.; Feyer, V.; Richter, R.; Coreno, M.; de Simone, M.; Prince, K. C.; Trofimov, A. B.; Gromov, E. V.; Zaytseva, I. L.; Schirmer, *J. Chem. Phys.* **2008**, *347*, 360.

(23) Samuel, N. T.; Lee, C.-J.; Gamble, L. J.; Fischer, D. A.; Castner, D. G. *J. Electron Spectrosc. Relat. Phenom.* **2006**, *152*, 134.

(24) Zubavichus, Y.; Shaporenko, A.; Korolkov, V.; Grunze, M.; Zharnikov, M. *J. Phys. Chem. B* **2008**, *112*, 13711.

(25) Harada, Y.; Takeuchi, T.; Kino, H.; Fukushima, A.; Kaoru, T.; Hieda, K.; Nakao, A.; Shin, S.; Fukuyama, H. *J. Phys. Chem. A* **2006**, *110*, 13227.

(26) MacNaughton, J.; Moewes, A.; Kurmaev, E. Z. *J. Phys. Chem. B* **2005**, *109*, 7749.

(27) Vyalikh, D. V.; Fedoseenko, S. I.; Iossifov, I. E.; Follath, R.; Gorovikov, S. A.; Schmidt, J.-S.; Molodtsov, S. L.; Adamchuk, V. K.; Gudat, W.; Kaindl, G. *Synch. Rad. News* **2002**, *15*, 26.

(28) Fedoseenko, S. I.; Vyalikh, D. V.; Iossifov, I. F.; Follath, R.; Gorovikov, S. A.; Püttner, R.; Schmidt, J.-S.; Molodtsov, S. L.; Adamchuk, V. K.; Gudat, W.; Kaindl, G. *Nucl. Instrum. Methods Phys. Res. A* **2003**, *505*, 718.

(29) Vyalikh, D. V.; Danzenbächer, S.; Mertig, M.; Kirchner, A.; Pompe, W.; Dedkov, Yu.S.; Molodtsov, S. L. *Phys. Rev. Lett.* **2004**, *93*, 238103.

(30) Vyalikh, D. V.; Kirchner, A.; Danzenbächer, S.; Dedkov, Yu. S.; Kade, A.; Mertig, M.; Molodtsov, S. L. *J. Phys. Chem. B* **2005**, *109*, 18620.

(31) Kummer, K.; Vyalikh, D. V.; Gavrila, G.; Kade, A.; Weigel-Jech, M.; Mertig, M.; Molodtsov, S. L. *J. Electron Spectrosc. Relat. Phenom.* **2008**, *163*, 59.

(32) Kade, A.; Vyalikh, D. V.; Danzenbächer, S.; Kummer, K.; Blüher, A.; Mertig, M.; Lanzara, A.; Scholl, A.; Doran, A.; Molodtsov, S. L. *J. Phys. Chem. B* **2007**, *111*, 13491.

(33) Howells, M. R.; Hitchcock, A. P.; Jacobsen, C. J. *J. Electron Spectrosc. Relat. Phenom.* **2009**, *170*, 1–68.

(34) Siegbahn, K. *Rev. Mod. Phys.* **1982**, *54*, 709.

(35) Lee, C.-Y.; Gamble, L. J.; Grainger, D. W.; Castner, D. G. *Biointerphases* **2006**, *1*, 82.

(36) Lee, C.-Y.; Gong, P.; Harbers, G. M.; Grainger, D. W.; Castner, D. G.; Gamble, L. J. *Anal. Chem.* **2006**, *78*, 3316.

(37) Takahata, Y.; Okamoto, A. K.; Chong, D. P. *Int. J. Quantum Chem.* **2006**, *106*, 2581.

(38) Hayakawa, M.; Yoshinari, M.; Nemoto, K. *J. Biomed. Mater. Res. A* **2003**, *67A*, 684.

(39) Fu, R.; Zheng, B.; Liu, J.; Weiss, S.; Ying, J. Y.; Dresselhaus, M. S.; Dresselhaus, G.; Satcher, J., Jr.; Baumann, T. *J. Appl. Polym. Sci.* **2004**, *91*, 3060.

(40) Brow, R. K.; Osborne, Z. A. *Surf. Interface Anal.* **1996**, *24*, 91.

(41) Juodkazis, K.; Juodkazyte, J.; Jasulaitiene, V.; Lukinskas, A.; Sebeka, B. *Electrochem. Commun.* **2000**, *2*, 503.

(42) Wagner, C. D.; Zatko, D. A.; Raymond, R. H. *Anal. Chem.* **1980**, *52*, 1445.

(43) Yeh, J. J. *Atomic Calculation of Photoionization Cross-Sections and Asymmetry Parameters*; Gordon and Breach Science Publishers: Langhorne, PE (USA), 1993. Yeh, J. J.; Lindau, I. *At. Data Nucl. Data Tables* **1985**, *32*, 1.

(44) How strongly the counter ion will claim the surplus electron will certainly depend on the possible energy gain upon returning from the positively charged to the neutral state, which can be estimated from the respective ionization energies. Note the enhanced ionization energy of hydrogen (1312 kJ/mol) when compared to sodium (496 kJ/mol). Data taken from: Huheey, J. E.; Keiter, E. A.; Keiter, R. L. *Inorganic Chemistry: Principles of Structure and Reactivity*, 4th ed., Harper Collins: New York, USA, 1993. James, A. M.; Lord, M. P. *Macmillan's Chemical and Physical Data*; Macmillan: London, UK, 1992.

(45) Kick, A.; Bönsch, M.; Kummer, K.; Vyalikh, D. V.; Molodtsov, S. L.; Mertig, M. *J. Electron Spectrosc. Relat. Phenom.* **2009**, *172*, 36.

(46) Stöhr, J. *NEXAFS Spectroscopy*; Springer Series in Surface Science 25; Springer: Berlin, 1996; corr. 2nd printing, pp 179−185.

(47) Zwahlen, M.; Brovelli, D.; Caseri, W.; Hähner, G. *J. Colloid Interface Sci.* **2002**, *256*, 262.

(48) Kaznacheyev, K.; Osanna, A.; Jacobsen, C.; Plashkevych, O.; Vahtras, O.; Ågren, H.; Carravetta, V.; Hitchcock, A. P. *J. Phys. Chem. A* **2002**, *106*, 3153.

(49) Kummer, K.; Sivkov, V. N.; Vyalikh, D. V.; Maslyuk, V. V.; Blüher, A.; Nekipelov, S. V.; Bredow, T.; Mertig, I.; Mertig, M.; Molodtsov, S. L. *Phys. Rev. B* **2009**, *80*, 155433.

(50) Shard, A. G.; Whittle, J. D.; Beck, A. J.; Brookes, P. N.; Bullett, N. A.; Talib, R. A.; Mistry, A.; Barton, D.; McArthur, S. L. *J. Phys. Chem. B* **2004**, *108*, 12472.

(51) Moewes, A.; MacNaughton, J.; Wilks, R.; Lee, J. S.; Wettig, S. D.; Kraatz, H.-B.; Kurmaev, E. Z. *J. Electron Spectrosc. Relat. Phenom.* **2004**, *137*, 817.

(52) Gordon, M. L.; Cooper, G.; Morin, C.; Araki, T.; Turci, C. C.; Kaznatcheev, K.; Hitchcock, A. P. *J. Phys. Chem. A* **2003**, *107*, 6144.

(53) Urquhart, S. G.; Ade, H. *J. Phys. Chem. B* **2002**, *106*, 8531.

(54) Ohta, T.; Seki, K.; Yokoyama, T.; Morisada, I.; Edamatsu, K. *Phys. Scr.* **1990**, *41*, 150.

(55) Dannenberger, O.; Weiss, K.; Himmel, H.-J.; Jäger, B.; Buck, M.; Wöll, Ch. *Thin Solid Films* **1997**, *307*, 183.

(56) Hitchcock, A. P.; Ishii, I. *J. Electron Spectrosc. Relat. Phenom.* **1986**, *42*, 11.

(57) Outka, D. A.; Stöhr, J.; Rabe, J. P.; Swalen, J. D. *J. Chem. Phys.* **1988**, *88*, 4076. Outka, D. A.; Stöhr, J. *J. Chem. Phys.* **1988**, *88*, 3539.

(58) Hähner, G.; Kinzler, M.; Wöll, Ch.; Grunze, M.; Scheller, M. K.; Cederbaum, L. S. *Phys. Rev. Lett.* **1991**, *67*, 851.

(59) Bagus, R. S.; Weiss, K.; Schertel, A.; Wöll, Ch.; Braun, W.; Hellwig, C.; Jung, C. *Chem. Phys. Lett.* **1996**, *248*, 129.

(60) Weiss, K.; Bagus, P. S.; Wöll, Ch. *J. Chem. Phys.* **1999**, *111*, 6834.

(61) Fujii, K.; Yokoya, A. *Radiat. Phys. Chem.* **2009**, *78*, 1188.

(62) Furukawa, M.; Kato, H. S.; Taniguchi, M.; Kawai, T.; Hatsui, T.; Kosugi, N.; Yoshida, T.; Aida, M.; Kawai, M. *Phys. Rev. B* **2007**, *75*, 045119.

(63) Fujii, K.; Akamatsu, K.; Yokoya, A. *J. Phys. Chem. B* **2004**, *108*, 8031.

(64) Kirtley, S. M.; Mullins, O. C.; Chen, J.; van Elp, J.; George, S. J.; Chen, C. T.; O'Halloran, T.; Cramer, S. P. *Biochim. Biophys. Acta* **1992**, *1132*, 249.

(65) Mochizuki, Y.; Koide, H.; Imamura, T.; Takemiya, H. *J. Synchrotron Radiat.* **2001**, *8*, 1003.

(66) Fujii, K.; Akamatsu, K.; Muramatsu, Y.; Yokoya, A. *Nucl. Instr. Methods Phys. Res. B* **2003**, *199*, 249, and references therein.

(67) *Z* being the atomic number of the atoms contained in the molecule.

(68) Zhang, M.-L.; Miao, M. S.; Van Doren, V. E.; Ladik, J. J.; Mintmire, J. W. *J. Chem. Phys.* **1999**, *111*, 8696.

(69) Maslyuk, V. V.; Mertig, I.; Bredow, T.; Mertig, M.; Vyalikh, D. V.; Molodtsov, S. L. *Phys. Rev. B* **2008**, *77*, 045419.

(70) Ireta, J.; Galván, M.; Cho, K.; Joannopoulos, J. D. *J. Am. Chem. Soc.* **1998**, *120*, 9771.

(71) Brühwiler, P. A.; Karis, O.; Martensson, N. *Rev. Mod. Phys.* **2002**, *74*, 703.

(72) Kato, H. S.; Furukawa, M.; Kawai, M.; Taniguchi, M.; Kawai, T.; Hatsui, T.; Kosugi, N. *Phys. Rev. Lett.* **2004**, *93*, 086403.

(73) Vyalikh, D. V.; Maslyuk, V. V.; Blüher, A.; Kade, A.; Kummer, K.; Dedkov, Yu. S.; Bredow, T.; Mertig, I.; Mertig, M.; Molodtsov, S. L. *Phys. Rev. Lett.* **2009**, *102*, 098101.

JP1013237